

Parmbsc1: a refined force field for DNA simulations

Ivan Ivani^{1,2}, Pablo D Dans^{1,2}, Agnes Noy³, Alberto Pérez⁴, Ignacio Faustino^{1,2}, Adam Hospital^{1,2}, Jürgen Walther^{1,2}, Pau Andrió^{2,5}, Ramon Goñi^{2,5}, Alexandra Balaceanu^{1,2}, Guillem Portella^{1,2,6}, Federica Battistini^{1,2}, Josep Lluis Gelpí^{2,7}, Carlos González⁸, Michele Vendruscolo⁶, Charles A Laughton^{9,10}, Sarah A Harris³, David A Case¹¹ & Modesto Orozco^{1,2,7}

We present parmbsc1, a force field for DNA atomistic simulation, which has been parameterized from high-level quantum mechanical data and tested for nearly 100 systems (representing a total simulation time of ~140 μs) covering most of DNA structural space. Parmbsc1 provides high-quality results in diverse systems. Parameters and trajectories are available at <http://mmb.irbbarcelona.org/ParmBSC1/>.

The force field, the energy functional used to describe the dependence between system conformation and energy, is the core of any classical simulation including molecular dynamics (MD). Its development is tightly connected to the extension of simulation timescales: as MD trajectories are extended to longer timescales, errors previously undetected in short simulations emerge, creating the need to improve the force field¹. For example, AMBER (Assisted Model Building with Energy Refinement) parm94-99 was the most used force field in DNA simulations until multi-nanosecond simulations revealed severe artifacts^{2,3}, fueling the development of parmbsc0 (ref. 4), which in turn started to show deviations from experimental data in the microsecond regime (for example, underestimation of twist, deviations in sugar puckering, biases in ϵ and ζ torsions, excessive terminal fraying^{2,5} and severe problems in representing certain noncanonical DNAs^{1,6}). Various force-field modifications have been proposed to address these problems, such as the Olomouc ones^{5,6} designed to reproduce specific forms of DNA. Although these and other tailor-made modifications are useful, there is an urgent need for a new general-purpose AMBER force field for DNA simulations to complement recent advances in the CHARMM (Chemistry at Harvard Macromolecular Mechanics) family of force fields

(Online Methods). We designed the parmbsc1 force field presented here to address these needs, with the aim of creating a general-purpose force field for DNA simulations. We assessed its performance by testing its ability to simulate a wide variety of DNA systems (Supplementary Table 1).

Parmbsc1 was able to fit quantum mechanical (QM) data well (Supplementary Discussion), improving on previous force-field results (Online Methods and Supplementary Table 2). We first tested QM-derived parameters on the Drew-Dickerson dodecamer (DDD), a well-studied DNA structure^{2,7} typically used as a benchmark in force-field development. Parmbsc1 trajectories sampled a stable B-type duplex that remained close to the experimental structures (Fig. 1 and Supplementary Table 2), preserving hydrogen bonds and helical characteristics even at the terminal base pairs, where fraying artifacts are common with other force fields^{2,8} (Online Methods and Supplementary Discussion). The average sequence-dependent helical parameters (Fig. 1 and Supplementary Figs. 1 and 2) and BI and BII conformational preferences (Supplementary Table 2 and Supplementary Fig. 3) matched experimental values (comparisons with estimates obtained with other force fields are presented in the Online Methods). Furthermore, parmbsc1 reproduced residual dipolar couplings (Q-factor = 0.3) and the nuclear Overhauser effect (NOE; only two violations), yielding success metrics similar to those obtained in the NMR-refined structures (Supplementary Table 3).

We next evaluated the ability of parmbsc1 to represent sequence-dependent structural features from simulations on 28 B-DNA duplexes (Supplementary Table 4). The agreement between simulation and experiment was excellent (r.m.s. deviation per base pair of 0.1 or 0.2 Å). Almost no artifacts arising from terminal fraying were present, and the average helical parameters (twist and roll from simulations of 33.9° and 2.5°, respectively) matched values from analyses of the RCSB Protein Data Bank (PDB) (33.6° and 2.9°) (ref. 9). Moreover, parmbsc1 was able to reproduce the unique properties of A-tract sequences¹⁰ (Supplementary Figs. 4–6) and capture sequence-dependent structural variability (Supplementary Fig. 7). We also studied longer duplexes (up to 56 bp) to ensure that a possible accumulation of small errors given by the force field did not compromise the description of the DNA, and we obtained excellent results (Supplementary Table 5). The expected spontaneous curvature was clearly visible in both static and dynamical descriptors, demonstrating that parmbsc1 trajectories were able to capture complex polymeric effects (Supplementary Table 5).

¹Institute for Research in Biomedicine (IRB) Barcelona, the Barcelona Institute of Science and Technology, Barcelona, Spain. ²Joint BSC-IRB Research Program in Computational Biology, IRB Barcelona, Barcelona, Spain. ³School of Physics and Astronomy, University of Leeds, Leeds, UK. ⁴Laufer Center for Physical and Quantitative Biology, Stony Brook University, Stony Brook, New York, USA. ⁵Barcelona Supercomputing Center, Barcelona, Spain. ⁶Department of Chemistry, University of Cambridge, Cambridge, UK. ⁷Department of Biochemistry and Molecular Biology, University of Barcelona, Barcelona, Spain. ⁸Instituto de Química Física 'Rocasolano', Consejo Superior de Investigaciones Científicas, Madrid, Spain. ⁹School of Pharmacy, University of Nottingham, Nottingham, UK. ¹⁰Centre for Biomolecular Sciences, University of Nottingham, Nottingham, UK. ¹¹Department of Chemistry and Chemical Biology, Rutgers University, Piscataway, New Jersey, USA. Correspondence should be addressed to M.O. (modesto.orozco@irbbarcelona.org).

RECEIVED 5 MAY; ACCEPTED 22 SEPTEMBER; PUBLISHED ONLINE 16 NOVEMBER 2015; DOI:10.1038/NMETH.3658

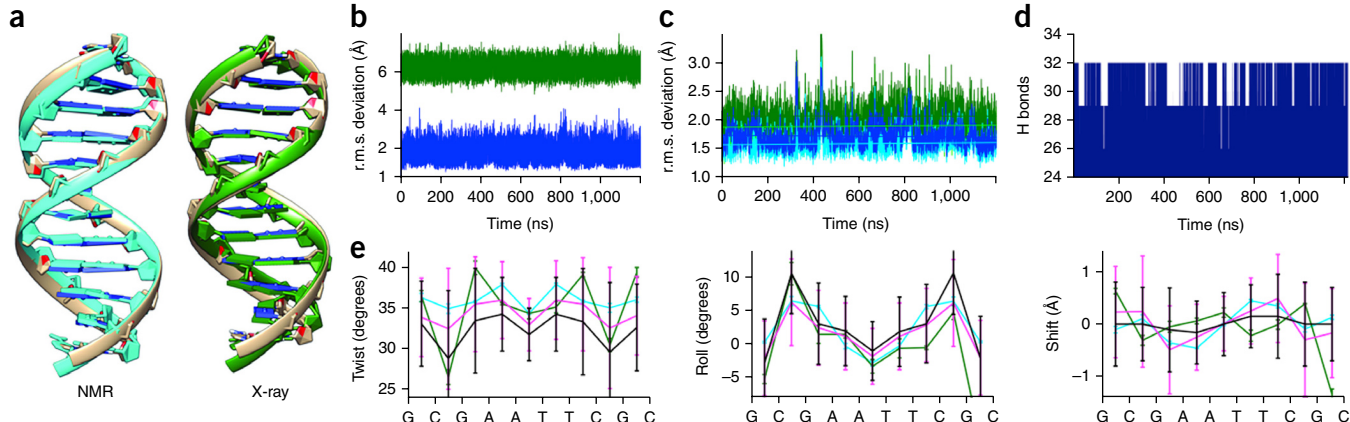


Figure 1 | Analysis of the DDD. (a) Comparison of the MD average structure (light brown) with the NMR structure (light blue) (PDB ID 1NAJ) and the X-ray structure (green) (PDB ID 1BNA). (b) r.m.s. deviation of 1.2- μ s trajectory of DDD compared with that for the B-DNA (blue) and A-DNA (green) forms (from the standard geometries derived from fiber diffraction (Online Methods)). (c) r.m.s. deviation of parmbsc1 data compared to experimental X-ray (green) and NMR (blue) structures (with (dark) and without (light) ending base pairs). Linear fits of all r.m.s. deviation curves are plotted on top. (d) Evolution of the total number of hydrogen bonds formed between base pairs in the whole duplex. (e) Comparison of average values of helical rotational parameters (twist, roll and shift) per base-pair step coming from NMR (cyan), X-ray (green), 1- μ s parmbsc0 trajectory² (black) and 1.2- μ s parmbsc1 trajectory (magenta) data. Error bars denote \pm s.d.

We also explored the ability of parmbsc1 to represent unusual DNA configurations, such as a Holliday junction, a complex duplex-quadruplex structure, which was fully preserved in microsecond-long trajectories (Supplementary Figs. 8 and 9), or Z-DNA, a *levo* duplex containing nucleotides in *syn*, for which parmbsc1 not only provided stable trajectories (Fig. 2a) but also reproduced the experimentally known salt dependence, confirming that the conformation is stable only at high (4 M) salt concentrations¹¹. For Hoogsteen DNA, simulations with parmbsc1 showed a stable duplex for more than 150 ns (Fig. 2b) and severe distortions in longer simulation periods (Supplementary Fig. 10), as expected from its metastable nature¹². We obtained equivalent results for another metastable structure, the parallel poly-d(AT) DNA¹³ (Supplementary Fig. 11). Parmbsc1 simulations not only reproduced the known structure of parallel d(T-A-T) and d(G-G-C) tripleplexes (Fig. 2c,d) but also showed correctly that the equivalent antiparallel structures are unstable in normal conditions¹⁴ (Fig. 2e). Finally, parmbsc1 was able to reproduce experimental structures of both parallel and antiparallel DNA quadruplexes with r.m.s. deviation of <2 \AA (Fig. 2f,g).

We also explored the ability of parmbsc1 to reproduce the complex conformations of hairpins and loops, exceptionally challenging

structures for force fields¹⁵. We performed microsecond simulations of the d(GCGAAGC) hairpin (PDB ID 1PQT), the 4T-tetraloop in *Oxytricha nova* quadruplex d(G₄T₄G₄)₂ (OxyQ; PDB ID 1JRN) and the junction loops in the human telomeric quadruplex (HTQ; PDB ID 1KF1). Parmbsc1 provided excellent representations (r.m.s. deviation of ~ 1 \AA) of the d(GCGAAGC) hairpin (Fig. 2h) and OxyQ (Fig. 2i). For the very challenging HTQ structure, parmbsc1 maintained the stem structure 20 times longer than in previous

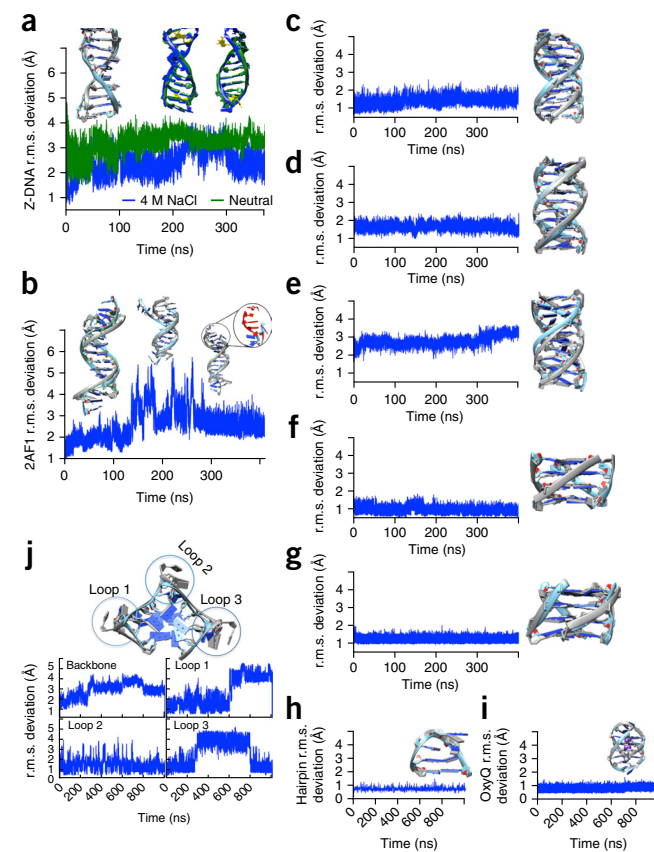


Figure 2 | Analysis of noncanonical DNA structures. (a) Comparison of Z-DNA (PDB ID 1IOT) simulations in neutral conditions and in 4 M NaCl. Structural comparisons at different time points are shown above the r.m.s. deviation curves. (b) Simulation of anti-parallel Hoogsteen DNA (PDB ID 2AF1) showing deviation of the structure over time (highlighted in red). (c-e) r.m.s. deviation of (c) parallel d(T-A-T)₁₀, (d) parallel d(G-G-C)₁₀ and (e) antiparallel d(G-G-C)₁₀ tripleplexes. (f,g) Parallel (f) (PDB ID 352D) and anti-parallel (g) (PDB ID 156D) quadruplexes showed stable structures over time. (h) Structural stability of d(GCGAAGC) hairpin (PDB ID 1PQT) and (i) OxyQ (PDB ID 1JRN) with ions over time. (j) HTQ (PDB ID 1KF1) with highlighted loops. r.m.s. deviations of HTQ backbone, loop 1, loop 2 and loop 3 regions are shown below. In all panels, parmbsc1 structures (light blue; final, averaged or at a given trajectory point) overlap the experimental structure (gray) for comparison. Green shading in structures denotes Z-DNA. **Supplementary Table 1** presents information on the PDB structures.

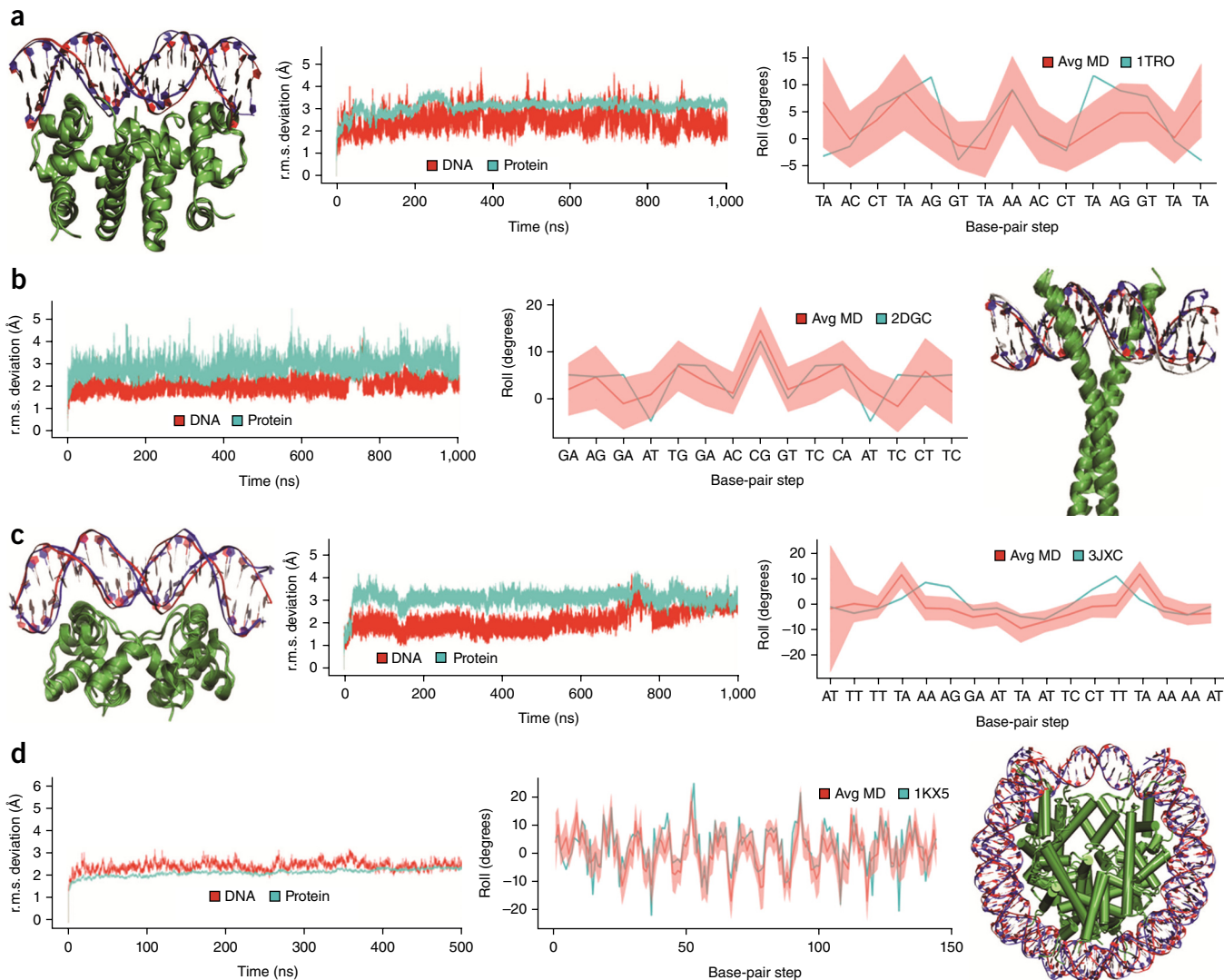


Figure 3 | Analysis of DNA-protein complexes. (a–d) Structural details of microsecond trajectories of four complexes: PDB IDs 1TRO (a), 2DGC (b), 3JXC (c) and 1KX5 (d) (500-ns trajectory). Each panel shows the overlap of the MD starting (red) and final (blue) structures, the protein secondary structure (green), the time-dependent mass-weighted r.m.s. deviation of all DNA and protein heavy atoms, and a comparison of the rotational helical parameter roll at each base-pair step calculated from the X-ray crystal structure and averaged along the MD simulation (Avg MD) (the s.d. envelope is shown in light red). For clarity, in the roll plot for 1KX5 (d), the base-pair steps are defined by the position along the DNA strand, and not by the base pair.

simulations¹⁵ and recognized the considerable flexibility of the loops in the absence of the lattice contacts (Supplementary Fig. 12), showing that, as predicted¹⁶, not only the crystal but also other loop conformations were sampled (Fig. 2j).

As an additional, critical test of the new force field, we predicted NMR observables from parmbsc1 trajectories (Online Methods). We obtained NOE violation statistics equivalent to those determined from NMR-derived ensembles (Supplementary Tables 6 and 7 and Supplementary Fig. 13). This agreement was maintained in *de novo* predictions (i.e., in those cases where NMR observables were collected in one of our laboratories after parmbsc1 development; Supplementary Table 8). Finally, it is worth noting that parmbsc1 trajectories reproduced the structure of DNA in crystal environments, yielding an r.m.s. deviation between the simulated and crystal structures of only 0.7 Å and average twist differences of <1°, representing improvements on previous calculations (Online Methods and Supplementary Figs. 14 and 15).

In our final structural test, we explored the ability of parmbsc1 to reproduce the conformation of DNA in complex with other molecules. We studied four diverse protein-DNA complexes (PDB IDs 1TRO, 2DGC, 3JXC and 1KX5) and two prototypical drug-DNA complexes. In all cases, we found excellent agreement with experiments (r.m.s. deviation for DNA of about 2–3 Å in protein-DNA complexes and 1–2 Å in drug-DNA complexes) (Fig. 3 and Supplementary Figs. 16 and 17).

A force field should reproduce not only the structure of DNA but also its mechanical properties¹. To evaluate the performance of parmbsc1, we first evaluated the microsecond-scale dynamics of the central 10 bp of the DDD. The agreement between parmbsc0 and parmbsc1 normal modes and entropy estimates (Online Methods and Supplementary Table 9) demonstrated that parmbsc1 did not ‘freeze’ the DNA structure, a risk for a force field reproducing average properties. This was further confirmed by the ability of parmbsc1 to reproduce the DNA

dielectric constant (8.0 ± 0.3 for DDD versus the experimental estimate of 8.5 ± 1.4 ; **Supplementary Fig. 18**) and the cooperative binding ($\sim 0.7 \text{ kcal mol}^{-1}$) of Hoechst 33258 to DNA. We then computed the helical-stiffness matrices for the ten unique base-pair steps^{17,18}. Parmbsc1 values were intermediate between parmbsc0 and CHARMM27 stiffness parameters¹⁸ and were substantially smaller than those suggested by Olson *et al.*¹⁷ (**Supplementary Table 10** and **Supplementary Fig. 19**); the dependence of the stiffness parameters on sequence was similar for parmbsc1 and parmbsc0 (ref. 17).

The persistence length and the torsional and stretching modules were obtained from simulations of long (up to 56 bp) duplexes (Online Methods). Parmbsc1 predicted persistence lengths in the range of 40–57 nm (**Supplementary Table 11**), close to the generally accepted value of 50 nm. The computed static persistence length, stretch and twist torsion modules were about 500 nm, 1,100–1,500 pN and 50–100 nm, respectively, also in agreement with experimental values (**Supplementary Table 11**). Finally, we explored the ability of parmbsc1 to describe relaxed and stressed DNA minicircles. We performed three 100-ns simulations of a 106-bp minicircle with ten turns (106t10), which should have zero superhelical density ($\sigma = 0$) and therefore no denatured regions^{19,20} (**Supplementary Fig. 20**). We observed a kink in only a single replica for one of the register angles, and in the remaining simulations the DNA remained intact (**Supplementary Fig. 20**). In contrast, negatively supercoiled 100-bp (100t9; $\sigma = -0.05$) and 106-bp (106t9; $\sigma = -0.10$) minicircles formed distortions as a result of the superhelical stress, as previously determined experimentally in studies using enzymes that digest single-stranded DNA^{19,20}.

Having demonstrated the ability of parmbsc1 to describe stable and metastable DNA structures and DNA flexibility, we finally studied conformational transitions. Parmbsc1 reproduced the spontaneous A-to-B-form DNA transition in water, and as expected, the A form was found to be stable in 200-ns control simulations in a mixture of 85% ethanol and 15% water (vol/vol) (**Supplementary Fig. 21**). Parmbsc1 also reproduced the unfolding of DNA d(GGCGGC)₂ in a 4 M pyridine solution (**Supplementary Fig. 21**) and the effective folding of d(GCGAAGC) in water (**Supplementary Fig. 22**), suggesting the ability to capture long-scale conformational changes in DNA.

On the basis of the wide series of tests reported here, we conclude that parmbsc1 provides good representations of the static and dynamic properties of DNA. We anticipate that parmbsc1 will be a valuable reference force field for atomistic DNA simulations under a diverse range of conditions. Parameters (**Supplementary Software**) and trajectories are available at <http://mmb.irbbarcelona.org/ParmBSC1/>.

METHODS

Methods and any associated references are available in the [online version of the paper](#).

Note: Any Supplementary Information and Source Data files are available in the online version of the paper.

ACKNOWLEDGMENTS

M.O. thanks the Spanish Ministry of Science (BI02012-32868), the Catalan SGR, the Instituto Nacional de Bioinformática and the European Research Council (ERC SimDNA) for support. M.O. is an academia researcher in the Catalan Institution for Research and Advanced Studies (ICREA). M.O. thanks the Barcelona Supercomputing Center for CPU and GPU time on MareNostrum and MinoTauro. C.A.L., S.A.H. and A.N. thank the UK HECBioSim Consortium for time on the ARCHER high-performance computing system (grant EP-L000253-1). A.N. was supported by the Biotechnology and Biological Sciences Research Council (BBSRC; grant BB-I019294-1) and thanks ARC Leeds for computational resources. P.D.D. is a PEDECIBA (Programa de Desarrollo de las Ciencias Básicas) and SNI (Sistema Nacional de Investigadores; ANII, Uruguay) researcher. D.A.C. thanks C. Liu for assistance with the crystal simulation analysis.

AUTHOR CONTRIBUTIONS

I.I. derived the parmbsc1 force-field parameter set. I.I., P.D.D., A.N., A.P., I.F., A.H., J.W., A.B., G.P., F.B., C.A.L. and S.A.H. performed validation simulations. C.G., M.V. and G.P. validated results from NMR-based experiments. C.G. obtained *de novo* NMR spectroscopy measurements. D.A.C. performed crystal MD simulations. R.G., P.A., A.H. and J.L.G. created the database infrastructure and web application. All authors contributed to data analysis. M.O. had the idea for the study, directed the project and wrote the manuscript, which was improved by the rest of the authors.

COMPETING FINANCIAL INTERESTS

The authors declare no competing financial interests.

Reprints and permissions information is available online at <http://www.nature.com/reprints/index.html>.

1. Pérez, A., Luque, F.J. & Orosco, M. *Acc. Chem. Res.* **45**, 196–205 (2012).
2. Pérez, A., Luque, F.J. & Orosco, M. *J. Am. Chem. Soc.* **129**, 14739–14745 (2007).
3. Várnai, P. & Zakrzewska, K. *Nucleic Acids Res.* **32**, 4269–4280 (2004).
4. Pérez, A. *et al.* *Biophys. J.* **92**, 3817–3829 (2007).
5. Zgarbová, M. *et al.* *J. Chem. Theory Comput.* **9**, 2339–2354 (2013).
6. Krepl, M. *et al.* *J. Chem. Theory Comput.* **8**, 2506–2520 (2012).
7. Wing, R. *et al.* *Nature* **287**, 755–758 (1980).
8. Lavery, R. *et al.* *Nucleic Acids Res.* **38**, 299–313 (2010).
9. Dans, P.D., Pérez, A., Faustino, I., Lavery, R. & Orosco, M. *Nucleic Acids Res.* **40**, 10668–10678 (2012).
10. Lankás, F., Špačková, N., Moakher, M., Enkhbayar, P. & Šponer, J. *Nucleic Acids Res.* **38**, 3414–3422 (2010).
11. Thamann, T.J., Lord, R.C., Wang, A.H.J. & Rich, A. *Nucleic Acids Res.* **9**, 5443–5458 (1981).
12. Abrescia, N.G.A., González, C., Gouyette, C. & Subirana, J.A. *Biochemistry* **43**, 4092–4100 (2004).
13. Cubero, E., Luque, F.J. & Orosco, M. *J. Am. Chem. Soc.* **123**, 12018–12025 (2001).
14. Soyfer, V.N. & Potaman, V.N. *Triple-helical Nucleic Acids* 1st edn. (Springer-Verlag, 1996).
15. Fadrná, E. *et al.* *J. Chem. Theory Comput.* **5**, 2514–2530 (2009).
16. Martín-Pintado, N. *et al.* *J. Am. Chem. Soc.* **135**, 5344–5347 (2013).
17. Olson, W.K., Gorin, A.A., Lu, X.-J., Hock, L.M. & Zhurkin, V.B. *Proc. Natl. Acad. Sci. USA* **95**, 11163–11168 (1998).
18. Pérez, A., Lankás, F., Luque, F.J. & Orosco, M. *Nucleic Acids Res.* **36**, 2379–2394 (2008).
19. Moroz, J.D. & Nelson, P. *Proc. Natl. Acad. Sci. USA* **94**, 14418–14422 (1997).
20. Du, Q., Kotlyar, A. & Vologodskii, A. *Nucleic Acids Res.* **36**, 1120–1128 (2008).

ONLINE METHODS

General parameterization strategy. AMBER charges and van der Waals parameters for DNA can be used to reproduce high-level QM data^{21–23} and hydration free energies^{24–26}, as well as to produce reasonable hydrogen-bond stabilities^{2,21–23,27} and complex properties such as sequence-dependent stability of duplex DNA^{2,28,29}. Thus we decided to keep the non-bonded parameters unaltered in this force-field revision and focus our efforts on parameterization of the backbone degrees of freedom: sugar puckering, glycosidic torsion, and ϵ and ζ rotations (taking the recently reparameterized α and γ torsions from parmbsc0 (ref. 4)). Parameterization of the different torsion angles (described below) was done from high-level QM calculations using the refined gas-phase fitted parameters as initial guesses for the refinement of parameters in solution, taken as reference high-level Self-Consistent Reaction Field (SCRF) QM data. In cases where fitting of one force-field parameter required knowledge of another parameter for optimization, we used an iterative procedure with parmbsc0 parameters in the first iteration.

QM calculations. Model compounds (Supplementary Fig. 23) were first geometrically optimized at the B3LYP/6-31++G(d,p) level³⁰, and from these single-point energies were calculated at the MP2/aug-cc-pVDZ level³¹. To minimize errors in the fitting, we performed optimizations while selected backbone and sugar dihedral angles were constrained to typical values obtained from a survey of DNA crystal structures⁹. We obtained both vacuum and solvent profiles for all structures calculated. 3D profiles of ϵ and ζ were sampled at 10° increments in the region of interest ($\epsilon = (175^\circ, 275^\circ)$, $\zeta = (220^\circ, 330^\circ)$) and at 40° increments in the rest of the profile. Profiles of χ were sampled at 15° increments and profiles of sugar pucker were sampled at 10° increments in the range of phase angles from 0° to 180°, and considering the four nucleosides. To increase the accuracy of the profiles, we performed CCSD(T)-complete basis set (CBS) calculations^{32,33} on key points along the potential energy surface (for ϵ and ζ , these points were the B_I, B_{Trans} and B_{II} states; χ minima of *anti* and *syn* regions, and maxima between them; and minima of North, East and South conformations for the sugar pucker). These calculations entailed optimization at the MP2/aug-cc-pVDZ level followed by single-point calculations at the MP2/aug-cc-pVXZ (X = triplex and quadruplex) levels. We obtained CBS energies by extrapolating to an infinite basis set, from the scheme of Halkier *et al.*³², and adding the correction term of the difference from CCSD(T) and MP2 with the 6-31+G(d) basis set. These high-level points were introduced with increased weights in the global fitting (described below). All QM calculations were performed with Gaussian09 (<http://www.gaussian.com>).

Solvent corrections in QM calculations. The solvent calculations were done at the single-point level using our version of the polarizable continuum model from Miertus, Scrocco and Tomasi (MST)^{34–40}. For comparison, test calculations were performed using the Cramer and Truhlar SMD (solvent model based on density)⁴¹ and standard integral equation formalism (IEF)-PCM³⁶ as implemented in the Gaussian09 package, which yielded very similar results (data not shown). Consequently, only MST values were used in this work.

Molecular mechanics and potential of mean force. Molecular mechanics (MM) reference calculations for the QM-optimized structures *in vacuo* were obtained from MM single-point energy calculations carried out with the AMBER 11 package (<http://www.ambermd.org>). MM profiles in solution were recovered from potential of mean force (PMF) calculations created with umbrella sampling (US)⁴² procedures in explicit solvent conditions (no restraints were used on any dihedrals out of the reaction coordinate in these calculations). US calculations were carried out with a weak biasing harmonic potential of 0.018 kcal mol⁻¹ deg⁻². The resulting populations were integrated using the Weighted Histogram Analysis Method (<http://membrane.urmc.rochester.edu/content/wham>). US calculations typically involve 40–100 windows, each consisting of 2–5 ns of equilibration and sampling times on the order of 1–2 ns. Simulation details in PMF-US calculations were the same as those outlined below for the validation of MD simulations.

Force-field fitting. The procedure for force-field fitting was similar to the parmbsc0 parameterization process⁴. To avoid altering other torsional parameters of the general force field, we introduced new atom types depending on the parameterization. For ϵ , ζ and sugar pucker parameterization, we assigned the atom type CE to the C3' atom. For χ parameterization, we assigned C1 to the C8 atom of adenine and C2 to the C6 atom of thymine, while keeping unchanged the atom types CK for guanine and CM for cytosine. Charges for model systems used in the parameterization were calculated via standard RESP methods mimicking the original AMBER parameterization. We used the standard torsion definitions $\epsilon = \text{C4}'\text{-C3}'\text{-O3}'\text{-P}$, $\zeta = \text{C3}'\text{-O3}'\text{-P-O5}'$, $\chi = \text{O4}'\text{-C1}'\text{-N9-C8}$ (for dA and dG) and $\chi = \text{O4}'\text{-C1}'\text{-N1-C6}$ (for dC and dT). For sugar pucker parameterization, we chose $v_1 = \text{O4}'\text{-C1}'\text{-C2}'\text{-C3}'$, the δ backbone and the $v_2 = \text{C1}'\text{-C2}'\text{-C3}'\text{-C4}'$ dihedrals, as they connect the two corrections: ϵ/ζ and χ (refs. 43–45).

As in the parmbsc0 parameterization, we used a Monte Carlo method for fitting residual energy, or QM-MM difference (equation (1)), to a Fourier series limited to the third order to maintain the AMBER force-field philosophy (equation (2)). The rotational barrier V_n and the phase angle α of each periodicity ($n = 1, 2, 3$) were fitted to obtain the minimal error in

$$E_{\text{dih},x} = E_{\text{QM}} - E_{\text{ffbsc0}(x=0)} \quad (1)$$

where x stands for a specific torsion or combination of torsions (in the case of ϵ and ζ) and $\text{ffbsc0}(x=0)$ refers to the standard parameters and the specific x torsion set to zero (used in reference MM or US calculations noted above). The dihedral term was defined as

$$E_{\text{dih}} = \sum_{\text{torsions}} \sum_n^3 \frac{V_n}{2} [1 + \cos(n\varphi - \alpha)] \quad (2)$$

where n stands for the periodicity of the torsion, V_n is the rotational barrier, φ is the torsion angle and α is the phase angle.

Our flexible Metropolis Monte Carlo algorithm allows for the introduction of different weights in the fitting for each point of the profile, as well as weighting of energy slopes to guarantee smooth transitions, or even mixing of information from different

profiles obtained in different conditions or with different levels of QM data. Fittings were done taking all the data into consideration, but with increased weighting at the profile minima (typically five times more than others) specially at the key points computed through the most accurate CCSD(T)-CBS approach (typically weighted nine times more than others). For certain cases such as sugar puckering, detailed attention was needed to properly reproduce the transition region, which we did by increasing the importance of the energy maximum and introducing weights to the slopes in the calculations (**Supplementary Figs. 24–26**). As described before⁴, around five to ten acceptable solutions of the Monte Carlo refinement were tested on short MD simulations (~50–100 ns) for one small duplex d(CGATCG)₂, rejecting those leading to distorted structures. The optimum parameter set (**Supplementary Discussion** and **Supplementary Table 12**), without additional refinement, was extensively tested against experimental data. Note that the way in which the parameters were derived does not guarantee their validity for RNA simulations, for which the use of other, already validated RNA force fields is recommended⁴⁵.

Validation of MD simulations. We performed MD simulations with the PMEMD code from AMBER 11-12 (<http://www.ambermd.org>) or with GROMACS⁴⁶, depending on the simulation. As shown in **Supplementary Figure 27**, results were insensitive to the simulation engine and to the use of CPU- or GPU-adapted codes⁴⁷. Unless otherwise noted, normal temperature and pressure conditions with default temperature and pressure settings at 300 K and 1 atm, respectively, were used. Calculations used an integration step of 2 fs in conjunction with SHAKE⁴⁸ (or LINCS⁴⁹ in the case of GROMACS) to constrain X-H bonds with the default values. We used the TIP3P⁵⁰ or SPCE⁵¹ water model with a minimum 10-Å buffer solvation layer beyond the solute, and we neutralized negatively charged DNA with Na⁺ or K⁺ ions⁵². Test simulations with added salt (NaCl) showed that DNA helical conformations were not strongly dependent on the surrounding ionic strength in the range of 0–0.5 M (**Supplementary Discussion** and **Supplementary Fig. 28**). Long-range electrostatic interactions were calculated using the particle mesh Ewald method⁵³ with default grid settings and tolerance. All structures were first optimized, thermalized and pre-equilibrated for 1 ns using our standard protocol⁸ and subsequently equilibrated for an additional 10-ns period. Conformational snapshots were saved every 1, 10, 20 or even 100 ps depending on the system size, the objective of the simulation and its length. Simulations mimicking crystal environments were carried out as described elsewhere⁵⁴ for d(CGATCGATCG)₂ (PDB ID **1D23**) using 2-μs simulations with 12 unit cells (or 32 duplexes) in the simulation periodic box (**Supplementary Fig. 14**) for a total of 64 μs of duplex simulation.

For annotation of conformational regions at the nucleotide level, we used standard criteria for sugar puckering (C3'-endo for P between 0° and 36° (canonical North), C4'-exo for P between 36° and 72°, O4'-endo for P between 72° and 108° (canonical East), C1'-exo for P between 108° and 144°, C2'-endo for P between 144° and 180° (canonical South), C3'-exo for P between 180° and 216°, C4'-endo for P between 216° and 252°, O4'-exo for P between 252° and 288° (canonical West), C1'-endo for P between 288° and 324°, and C2'-exo for P between 324° and 360°), glycosidic torsion

(*anti* for 90° to 180° or -60° to -180° and *syn* for -60° to 90°), BI (ϵ *trans*, ζ gauche-) and BII (ϵ gauche-, ζ *trans*). An H bond was annotated using standard GROMACS rules and was considered broken when the donor-acceptor distance was greater than 3.5 Å for at least ten consecutive picoseconds. Reference A-DNA and B-DNA fiber conformations were taken from Arnott's values⁵⁵. Whenever possible, the simulations were validated against experimental data obtained in solution.

We performed a variety of analyses to characterize the mechanical properties of DNA on the basis of MD simulations. For flexibility analysis we used essential dynamics algorithms^{56–58}, base-step stiffness analysis^{17,59,60} and quasi-harmonic entropies computed with either Andricioaei-Karplus⁶¹ or Schlitter⁶² procedures. We determined similarities between essential deformation movements using standard Hess metrics⁶³ as well as energy-corrected Hess metrics⁵⁹. We calculated polymer deformation parameters (persistence length, stretch and twist torsion modules) by means of different approaches in order to minimize errors associated with the use of a single method to move from atomistic simulations to macroscopic descriptors: (i) extrapolation of base-step translations and rotations^{17,59}, (ii) analysis of the correlations in the conformations and fluctuations of the DNA at different lengths⁶⁴ and (iii) implementation of Olson's hybrid approach, which required additional Monte Carlo simulations using MD-derived stiffness matrices⁶⁵. We computed dielectric constants of DNA using Pettit's procedure^{66,67}. We used the DDD sequence to compare parmbsc1 to other modern force fields (**Supplementary Discussion** and **Supplementary Fig. 29**). We paid special attention to fraying of the terminal base pairs when analyzing MD trajectories (**Supplementary Fig. 30**) and *de novo* NMR experiments (below and **Supplementary Fig. 31**).

We analyzed the trajectories using AMBERTOOLS (<http://www.ambermd.org>), GROMACS⁴⁶, MDWeb⁶⁸, NAFlex⁶⁹ and Curves+ (ref. 70), as well as with in-house scripts (<http://mmb.irbbarcelona.org/www/tools>).

NMR analysis. We analyzed the ability of MD trajectories to reproduce NMR observables (NOE-derived interatomic distances and residual dipolar couplings) using the last 950 ns of microsecond trajectories. We used the single-value decomposition method implemented in the program PALES⁷¹ to obtain the orientation tensor that best fit the calculated and observed residual dipolar coupling values. Violations of the NOE data were computed using the tool g_disre, included in the GROMACS package, using distance restraints derived from the deposited BioMagResBank database⁷², or as described below when NOEs were collected *de novo* using full relaxation matrix experiments.

The *novel* NMR experiments. Samples (3 mM oligonucleotide concentration) were suspended in 500 μL of either D₂O or H₂O-D₂O 9:1 in 25 mM sodium phosphate buffer, 125 mM NaCl, pH 7. NMR spectra were acquired in Bruker spectrometers operating at 800 MHz and processed with Topspin software. Double quantum filter correlation spectroscopy, total correlation spectroscopy and NOE spectroscopy (NOESY) experiments were recorded in D₂O and H₂O-D₂O 9:1. The NOESY spectra were acquired with mixing times of 75, 100, 200 and 300 ms, and the total correlation spectra were recorded with a standard MLEV-17 spin-lock sequence and 80-ms mixing time. NOESY spectra were recorded at 5 °C and 25 °C.

We used the spectral-analysis program Sparky (<https://www.cgl.ucsf.edu/home/sparky>) for semi-automatic assignment of the NOESY cross-peaks and quantitative evaluation of the NOE intensities. We obtained quantitative distance constraints from NOE intensities by using a complete relaxation matrix analysis with the program MARDIGRAS⁷³. We estimated error bounds in the interprotonic distances by carrying out several MARDIGRAS calculations with different initial models, mixing times and correlation times (2.0, 4.0 and 6.0 ns). We obtained final constraints by averaging the upper and lower distance bounds in all the MARDIGRAS runs.

Availability of force-field parameters and porting to different MD codes. The refined parameters were incorporated in AMBER-format libraries accessible from <http://mbb.irbbarcelona.org/ParmBSC1/>. Porting to GROMACS format was done from AMBER topology files using external utilities (amb2gmx⁷⁴ and acpype⁷⁵ tools accessible at <https://simtk.org/home/mmttools> and <https://github.com/choderalab/mmttools>). Porting to NAMD (<http://www.ks.uiuc.edu/Research/namd>) was not required because direct reading of AMBER topology files was possible.

Data management. We placed trajectories and the analysis performed in a novel dual-database framework for nucleic acid simulations, using Apache's Cassandra to manage trajectory data and MongoDB to manage trajectory metadata and analysis. Results are available at <http://mbb.irbbarcelona.org/ParmBSC1/>. Details on the nucleic acid database will be presented elsewhere.

21. Šponer, J., Jurecka, P. & Hobza, P. *J. Am. Chem. Soc.* **126**, 10142–10151 (2004).
22. Hobza, P., Kabeláč, M., Šponer, J., Mejzlík, P. & Vondrášek, J. *J. Comput. Chem.* **18**, 1136–1150 (1997).
23. Šponer, J. *et al.* *Chemistry* **12**, 2854–2865 (2006).
24. Orozco, M. & Luque, F.J. *Chem. Phys.* **182**, 237–248 (1994).
25. Colominas, C., Luque, F.J. & Orozco, M. *J. Am. Chem. Soc.* **118**, 6811–6821 (1996).
26. Orozco, M., Cubero, E., Hernández, B., López, J.M. & Luque, F.J. in *Computational Chemistry: Reviews of Current Trends* Vol. 4 (ed. Leszczynski, J.) 191–225 (World Scientific Publishing, 1999).
27. Pérez, A. *et al.* *Chemistry* **11**, 5062–5066 (2005).
28. Beveridge, D.L. *et al.* *Biophys. J.* **87**, 3799–3813 (2004).
29. Portella, G., Germann, M.W., Hud, N.V. & Orozco, M. *J. Am. Chem. Soc.* **136**, 3075–3086 (2014).
30. Krishnan, R., Binkley, J.S., Seeger, R. & Pople, J.A. *J. Chem. Phys.* **72**, 650–654 (1980).
31. Woon, D.E. & Dunning, T.H. Jr. *J. Chem. Phys.* **98**, 1358–1371 (1993).
32. Halkier, A. *et al.* *Chem. Phys. Lett.* **286**, 243–252 (1998).
33. Halkier, A., Helgaker, T., Jørgensen, P., Klopfer, W. & Olsen, J. *Chem. Phys. Lett.* **302**, 437–446 (1999).
34. Miertuš, S., Scrocco, E. & Tomasi, J. *Chem. Phys.* **55**, 117–129 (1981).
35. Miertuš, S. & Tomasi, J. *Chem. Phys.* **65**, 239–245 (1982).
36. Cancès, E., Mennucci, B. & Tomasi, J. *J. Chem. Phys.* **107**, 3032–3041 (1997).
37. Bachs, M., Luque, F.J. & Orozco, M. *J. Comput. Chem.* **15**, 446–454 (1994).
38. Soteras, I., Curutchet, C., Bidon-Chanal, A., Orozco, M. & Luque, F.J. *J. Mol. Struct. THEOCHEM* **727**, 29–40 (2005).
39. Soteras, I., Forti, F., Orozco, M. & Luque, F.J. *J. Phys. Chem. B* **113**, 9330–9334 (2009).
40. Soteras, I., Orozco, M. & Luque, F.J. *J. Comput. Aided Mol. Des.* **24**, 281–291 (2010).
41. Marenich, A.V., Cramer, C.J. & Truhlar, D.G. *J. Phys. Chem. B* **113**, 6378–6396 (2009).
42. Torrie, G.M. & Valleau, J.P. *J. Comput. Phys.* **23**, 187–199 (1977).
43. Hart, K. *et al.* *J. Chem. Theory Comput.* **8**, 348–362 (2012).
44. Wu, Z., Delaglio, F., Tjandra, N., Zhurkin, V.B. & Bax, A. *J. Biomol. NMR* **26**, 297–315 (2003).
45. Zgarbová, M. *et al.* *J. Chem. Theory Comput.* **7**, 2886–2902 (2011).
46. Hess, B., Kutzner, C., Van Der Spoel, D. & Lindahl, E. *J. Chem. Theory Comput.* **4**, 435–447 (2008).
47. Galindo-Murillo, R., Roe, D.R. & Cheatham, T.E. III. *Nat. Commun.* **5**, 5152 (2014).
48. Ryckaert, J.-P., Ciccotti, G. & Berendsen, H.J.C. *J. Comput. Phys.* **23**, 327–341 (1977).
49. Hess, B., Bekker, H., Berendsen, H.J.C. & Fraaije, J.G.E.M. *J. Comput. Chem.* **18**, 1463–1472 (1997).
50. Jorgensen, W.L., Chandrasekhar, J., Madura, J.D., Impey, R.W. & Klein, M.L. *J. Chem. Phys.* **79**, 926–935 (1983).
51. Berendsen, H.J.C., Grigera, J.R. & Straatsma, T.P. *J. Phys. Chem.* **91**, 6269–6271 (1987).
52. Smith, D.E. & Dang, L.X. *J. Chem. Phys.* **100**, 3757–3766 (1994).
53. Darden, T., York, D. & Pedersen, L. *J. Chem. Phys.* **98**, 10089–10092 (1993).
54. Liu, C., Janowski, P.A. & Case, D.A. *Biochim. Biophys. Acta* **1850**, 1059–1071 (2015).
55. Arnott, S. & Hukins, D.W.L. *Biochem. Biophys. Res. Commun.* **47**, 1504–1509 (1972).
56. Orozco, M., Pérez, A., Noy, A. & Luque, F.J. *Chem. Soc. Rev.* **32**, 350–364 (2003).
57. Pérez, A. *et al.* *J. Chem. Theory Comput.* **1**, 790–800 (2005).
58. Amadei, A., Linssen, A. & Berendsen, H.J.C. *Proteins* **17**, 412–425 (1993).
59. Lankás, F., Šponer, J., Hobza, P. & Langowski, J. *J. Mol. Biol.* **299**, 695–709 (2000).
60. Noy, A., Perez, A., Lankas, F., Luque, F.J. & Orozco, M. *J. Mol. Biol.* **343**, 627–638 (2004).
61. Andricioaei, I. & Karplus, M. *J. Chem. Phys.* **115**, 6289–6292 (2001).
62. Schlitter, J. *Chem. Phys. Lett.* **215**, 617–621 (1993).
63. Hess, B. *Phys. Rev. E Stat. Phys. Plasmas Fluids Relat. Interdiscip. Topics* **62**, 8438 (2000).
64. Noy, A. & Golestanian, R. *Phys. Rev. Lett.* **109**, 228101 (2012).
65. Zheng, G., Czapla, L., Srinivasan, A.R. & Olson, W.K. *Phys. Chem. Chem. Phys.* **12**, 1399–1406 (2010).
66. Cuervo, A. *et al.* *Proc. Natl. Acad. Sci. USA* **111**, E3624–E3630 (2014).
67. Yang, L., Weerasinghe, S., Smith, P.E. & Pettitt, P.M. *Biophys. J.* **69**, 1519–1527 (1995).
68. Hospital, A. *et al.* *Bioinformatics* **28**, 1278–1279 (2012).
69. Hospital, A. *et al.* *Nucleic Acids Res.* **41**, W47–W55 (2013).
70. Lavery, R., Moakher, M., Maddocks, J.H., Petkeviciute, D. & Zakrzewska, K. *Nucleic Acids Res.* **37**, 5917–5929 (2009).
71. Zweckstetter, M. *Nat. Protoc.* **3**, 679–690 (2008).
72. Bernstein, F.C. *et al.* *Eur. J. Biochem.* **80**, 319–324 (1977).
73. Borgias, B.A. & James, T.L. *J. Magn. Reson.* **87**, 475–487 (1990).
74. Mobley, D.L., Chodera, J.D. & Dill, K.A. *J. Chem. Phys.* **125**, 084902 (2006).
75. Sousa da Silva, A.W. & Vranken, W.F. *BMC Res. Notes* **5**, 367 (2012).